ESI

Tailoring the coordination microenvironment of Zn(II) in a light-responsive coordination polymer system for molecular sensing and photodegradation performance

Yan Zhao,[a,b, c] Xing Zhou,* [a] Zheng-Yu Liu,[b] Jia-Jun Wang,[b] Bo Ding,[b] Gui-Xi Liu,[c] and En-Cui Yang,* [b]

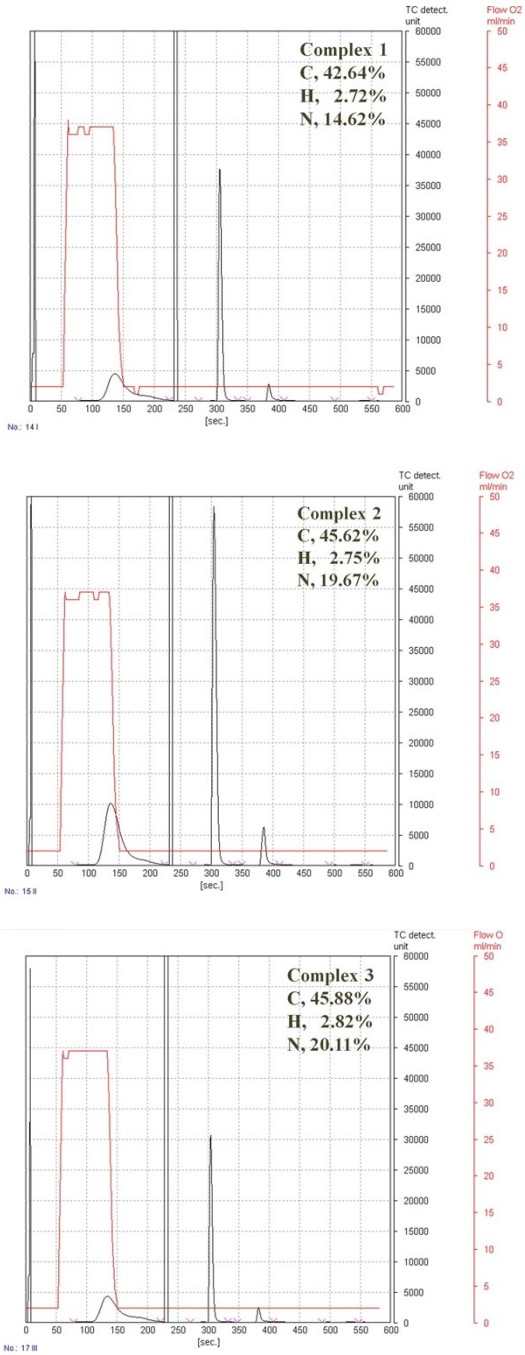

Fig. S1 The CHN analysis plots for **1–3**.

Table S1. Selected bond lengths and angles (Å, deg) for **1**.[a]

Cd(1)–O(10)	2.639(3)	Cd(2)–O(10)$^{\#1}$	2.327(3)
Cd(1)–O(11)	2.278(3)	Cd(2)–O(12)$^{\#2}$	2.212(2)
Cd(1)–O(16)	2.302(2)	Cd(2)–O(13)	2.185(3)
Cd(1)–O(17)	2.260(3)	Cd(2)–O(14)$^{\#3}$	2.352(2)
Cd(1)–N(5)	2.384(3)	Cd(2)–O(15)$^{\#3}$	2.429(3)
Cd(1)–N(6)	2.433(3)	Cd(2)–O(15)$^{\#4}$	2.391(2)
Cd(1)–N(8)	2.373(3)		
O(11)–Cd(1)–O(10)	52.81(8)	N(8)–Cd(1)–O(10)	89.03(10)
O(11)–Cd(1)–O(16)	92.21(10)	N(8)–Cd(1)–N(5)	68.86(11)
O(11)–Cd(1)–N(5)	149.72(10)	N(8)–Cd(1)–N(6)	136.12(11)
O(11)–Cd(1)–N(6)	82.47(10)	O(10)$^{\#1}$–Cd(2)–O(14)$^{\#2}$	82.54(9)
O(11)–Cd(1)–N(8)	141.27(10)	O(10)$^{\#1}$–Cd(2)–O(15)$^{\#2}$	88.35(9)
O(16)–Cd(1)–O(10)	80.65(10)	O(15)$^{\#3}$–Cd(2)–O(15)$^{\#2}$	72.72(10)
O(16)–Cd(1)–N(5)	85.41(11)	O(12)$^{\#4}$–Cd(2)–O(10)$^{\#1}$	81.70(9)
O(16)–Cd(1)–N(6)	87.83(10)	O(14)$^{\#2}$–Cd(2)–O(15)$^{\#2}$	54.84(9)
O(16)–Cd(1)–N(8)	87.07(10)	O(12)$^{\#4}$–Cd(2)–O(15)$^{\#3}$	83.93(8)
O(17)–Cd(1)–O(10)	92.23(9)	O(12)$^{\#4}$–Cd(2)–O(15)$^{\#2}$	104.49(9)
O(17)–Cd(1)–O(11)	88.43(10)	O(13)–Cd(2)–O(10)$^{\#1}$	118.86(10)
N(6)–Cd(1)–O(10)	132.85(10)	O(13)–Cd(2)–O(12)$^{\#4}$	111.39(9)
O(17)–Cd(1)–N(5)	98.78(11)	O(13)–Cd(2)–O(14)$^{\#2}$	93.99(10)
O(17)–Cd(1)–N(6)	101.67(10)	O(13)–Cd(2)–O(15)$^{\#3}$	88.24(10)
O(17)–Cd(1)–N(8)	86.49(10)	O(13)–Cd(2)–O(15)$^{\#2}$	137.11(9)
N(5)–Cd(1)–N(6)	67.29(11)	O(14)$^{\#2}$–Cd(2)–O(15)$^{\#3}$	101.42(8)

[a] Symmetry codes: $^{\#1}$ $-x, 2-y, -z$; $^{\#2}$ $-1-x, 2-y, -z$; $^{\#3}$ $+x, 1+y, +z$; $^{\#4}$ $-x, 3-y, -z$; $^{\#5}$ $+x, -1+y, +z$.

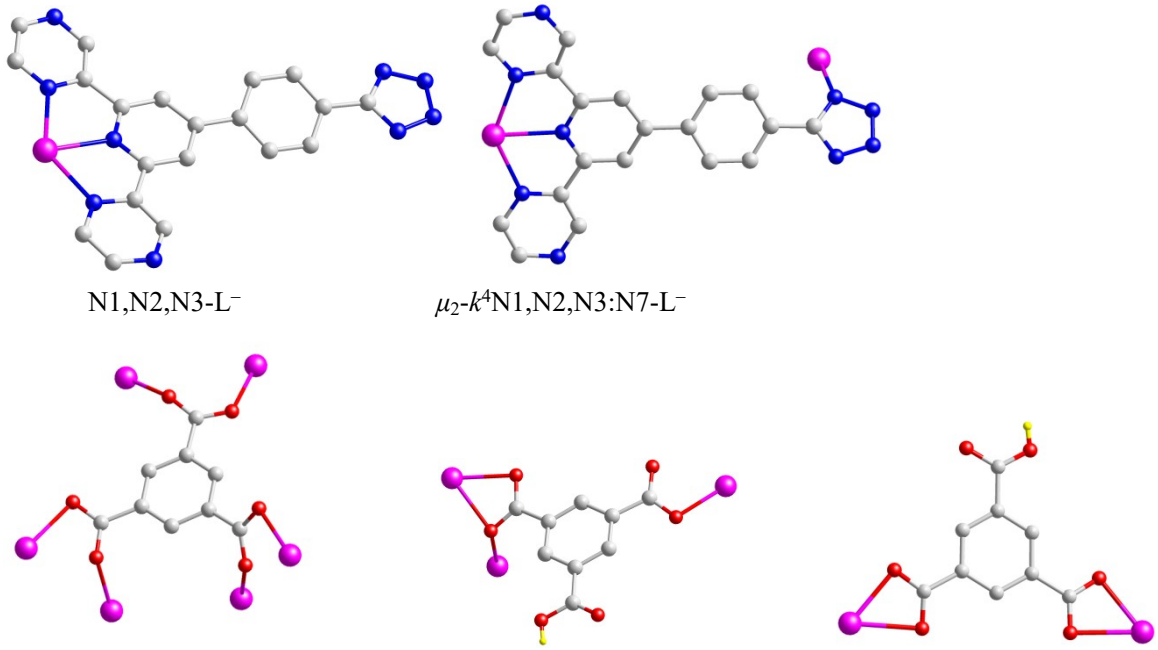

Fig. S2 Binding modes of L^-, $HBTC^{2-}$ and BTC^{3-} ligands in the ternary self-assembly system.

Table S2. Hydrogen-bonding parameters (Å, deg) for **1**–**3**.[a]

D–H···A	*d* (D–H)	*d* (H···A)	*d* (D···A)	∠DHA
1				
O(17)–H(17A)···N(2)	0.84	1.94	2.7458	160
O(17)–H(17B)···N(9)	0.84	2.00	2.8349	171
2				
O(7)–H(7B)···O(5)	0.85	1.94	2.7796	174
3				
O(3)–H(3A)···O(2)$^{\#1}$	0.85	1.917	2.7567	169
O(3)–H(3B)···N(8)$^{\#1}$	0.85	2.298	3.0030	140

[a] Symmetry code for **3**: $^{\#1}$ $-x$, $2-y$, $-z$.

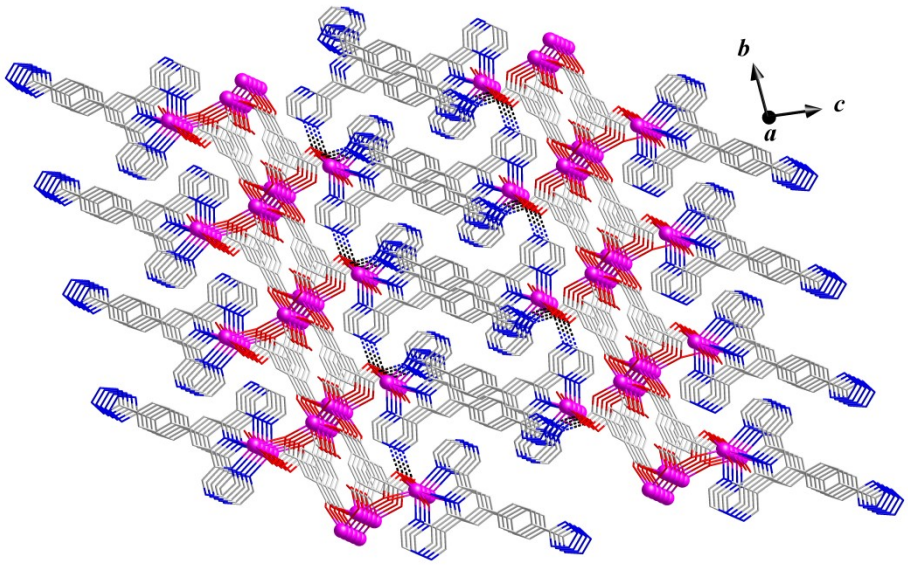

Fig. S3 3D supramolecular stacking of **1** by weak interlayer hydrogen-bonding interactions.

Table S3. Selected bond lengths and angles (Å, deg) for **2**.[a]

Cd(1)–N(3)	2.316(3)	Cd(2)–N(12)	2.352(3)
Cd(1)–N(9)$^{\#1}$	2.336(4)	Cd(2)–N(13)	2.360(3)
Cd(1)–O(1)	2.349(3)	Cd(2)–N(15)$^{\#3}$	2.362(4)
Cd(1)–N(4)	2.380(3)	Cd(2)–N(10)	2.391(3)
Cd(1)–N(1)	2.410(3)	Cd(2)–O(7)	2.432(3)
Cd(1)–O(2)	2.414(3)	Cd(2)–O(4)	2.183(3)
Cd(1)–O(2)$^{\#2}$	2.593(3)		
N(3)–Cd(1)–N(9)$^{\#1}$	108.48(11)	N(4)–Cd(1)–O(2)$^{\#2}$	88.52(10)
N(3)–Cd(1)–N(4)	69.37(10)	N(1)–Cd(1)–O(2)$^{\#2}$	85.11(10)
N(9)$^{\#1}$–Cd(1)–O(1)	82.56(11)	O(2)–Cd(1)–O(2)$^{\#2}$	75.02(9)
N(9)$^{\#1}$–Cd(1)–N(4)	109.34(13)	O(4)–Cd(2)–N(13)	136.92(11)
O(1)–Cd(1)–N(4)	83.59(10)	N(12)–Cd(2)–N(13)	68.65(10)
N(3)–Cd(1)–N(1)	69.45(10)	O(4)–Cd(2)–N(15)$^{\#3}$	92.63(11)
N(9)$^{\#1}$–Cd(1)–N(1)	85.06(12)	N(12)–Cd(2)–N(15)$^{\#3}$	102.31(11)
O(1)–Cd(1)–N(1)	137.41(10)	N(13)–Cd(2)–N(15)$^{\#3}$	85.49(13)
N(4)–Cd(1)–N(1)	138.80(10)	O(4)–Cd(2)–N(10)	85.09(10)
N(3)–Cd(1)–O(2)	146.69(9)	N(12)–Cd(2)–N(10)	68.65(10)
N(9)$^{\#1}$–Cd(1)–O(2)	88.01(11)	N(13)–Cd(2)–N(10)	137.29(10)
O(1)–Cd(1)–O(2)	55.14(9)	N(15)$^{\#3}$–Cd(2)–N(10)	102.86(12)
N(4)–Cd(1)–O(2)	133.24(10)	O(4)–Cd(2)–O(7)	86.94(11)
N(1)–Cd(1)–O(2)	83.91(9)	N(12)–Cd(2)–O(7)	86.11(10)
N(3)–Cd(1)–O(2)$^{\#2}$	82.88(9)	N(13)–Cd(2)–O(7)	82.26(11)
O(1)–Cd(1)–O(2)$^{\#2}$	93.98(9)	N(10)–Cd(2)–O(7)	95.57(10)

[a] Symmetry codes: $^{\#1}$ $-x+1, -y+2, -z$; $^{\#2}$ $-x+1, -y+1, -z$; $^{\#3}$ $-x+2, -y-1, -z+1$.

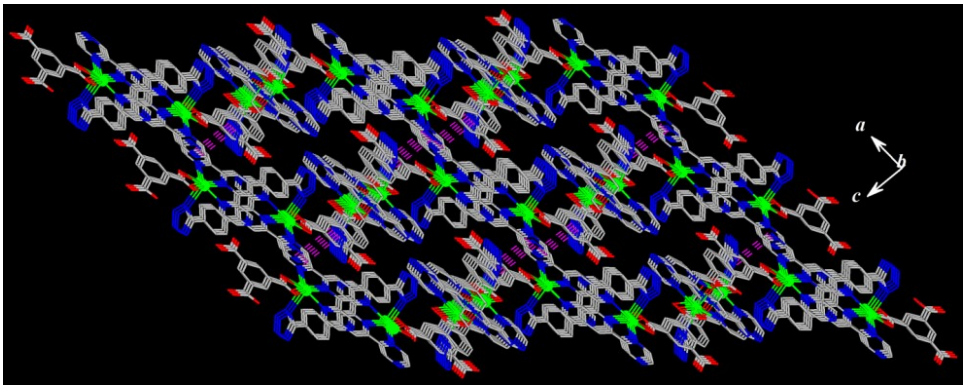

Fig. S4 3D stacking of **2** by weak intermolecular π···π and O–H···O interactions.

Table S4. Selected bond lengths and angles (Å, deg) for **3**.

Cd(1)–N(7)$^{\#1}$	2.309(2)	Cd(1)–O(3)	2.3923(17)
Cd(1)–N(3)	2.447(2)	Cd(1)–O(2)	2.3451(17)
Cd(1)–N(2)	2.3656(19)	Cd(1)–O(1)	2.4726(18)
Cd(1)–N(1)	2.392(2)		
N(7)$^{\#1}$–Cd(1)–O(2)	88.06(7)	N(1)–Cd(1)–N(3)	135.91(7)
N(7)$^{\#1}$–Cd(1)–N(2)	111.18(7)	O(3)–Cd(1)–N(3)	103.72(6)
O(2)–Cd(1)–N(2)	139.30(6)	N(7)$^{\#1}$–Cd(1)–O(1)	85.27(7)
N(7)$^{\#1}$–Cd(1)–N(1)	103.87(7)	O(2)–Cd(1)–O(1)	54.30(6)
O(2)–Cd(1)–N(1)	143.09(6)	O(2)–Cd(1)–N(3)	78.90(6)
N(2)–Cd(1)–N(1)	68.67(7)	N(1)–Cd(1)–O(1)	91.44(6)
N(7)$^{\#1}$–Cd(1)–N(3)	85.69(7)	O(3)–Cd(1)–O(1)	79.42(6)
O(2)–Cd(1)–O(3)	82.00(6)	N(3)–Cd(1)–O(1)	132.53(6)
N(2)–Cd(1)–O(3)	83.84(6)	N(1)–Cd(1)–O(3)	77.98(6)
N(2)–Cd(1)–N(3)	67.78(6)		

Symmetry codes: $^{\#1}$ $-x + 1/2, -y + 3/2, -z$; $^{\#2}$ $-x + 2, y, -z + 1/2$; $^{\#3}$ $-x, y, -z + 1/2$.

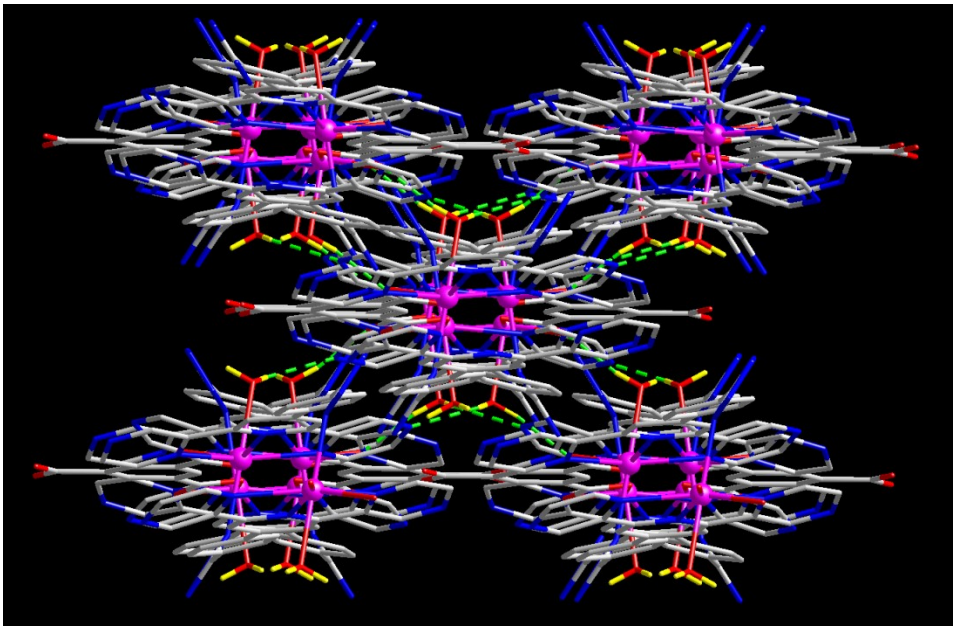

Fig. S5 3D stacking pattern of **3** by intermolecular hydrogen-bonding interactions.

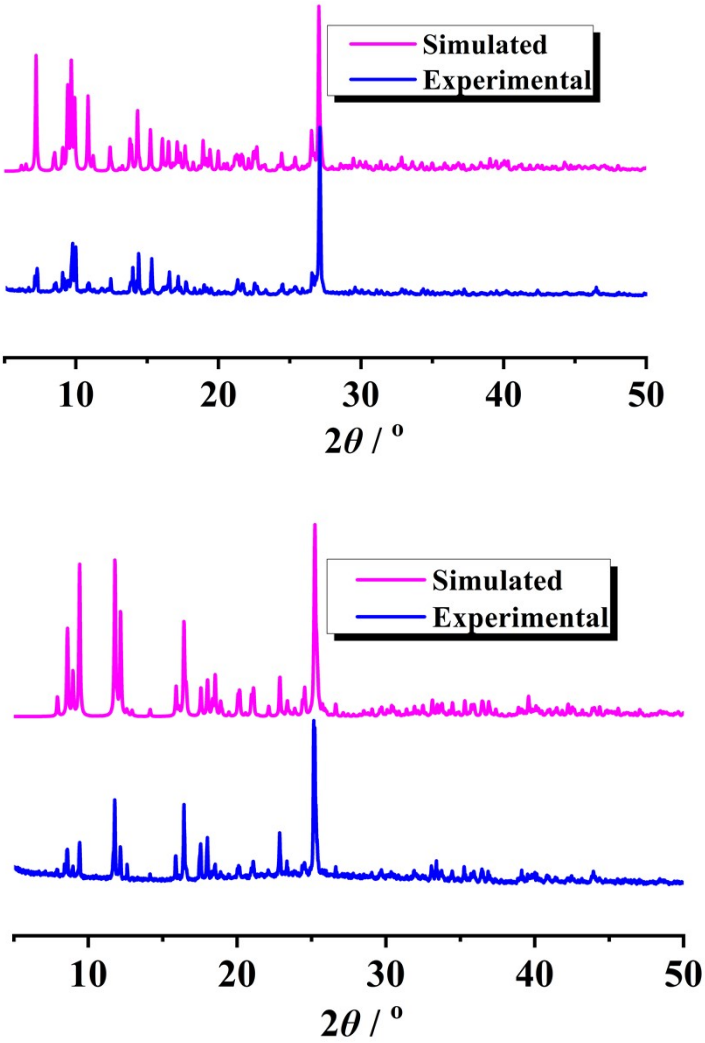

Fig. S6 Simulated and experimental PXRD patterns for **2** (upper) and **3** (bottom).

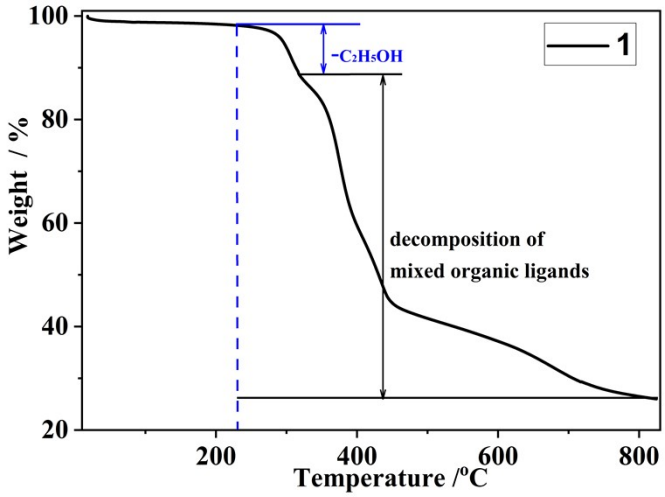

(a)

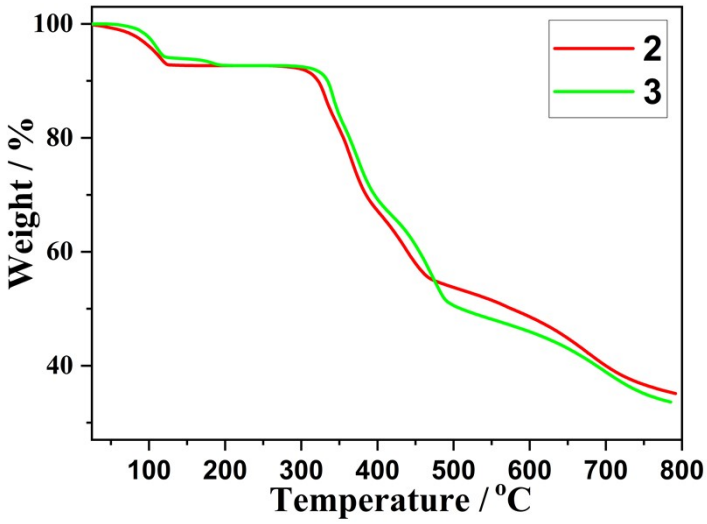

(b)

Fig. S7 TG curves for **1** – **3**.

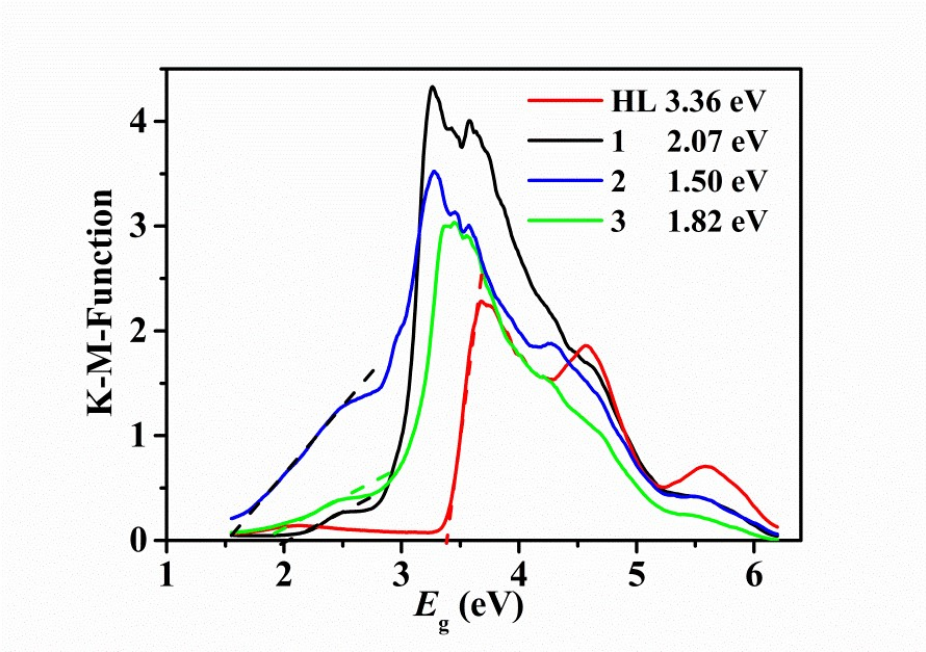

Fig. S8 Optical bandgaps for **1** – **3**.

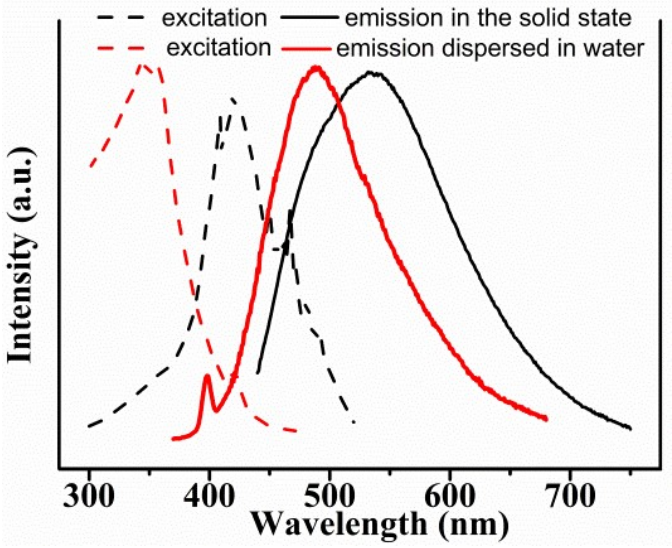

Fig. S9 Excitation and emission of **1** in the solid state and dispersed in water.

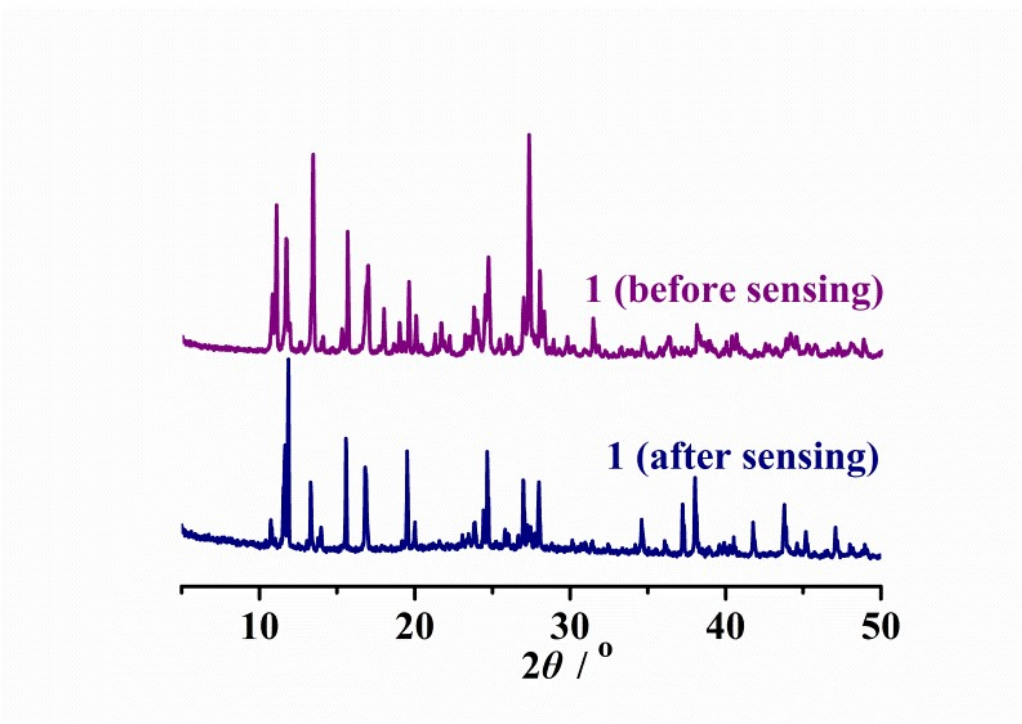

Fig. S10 PXRD patterns of **1** before and after bilirubin sensing.

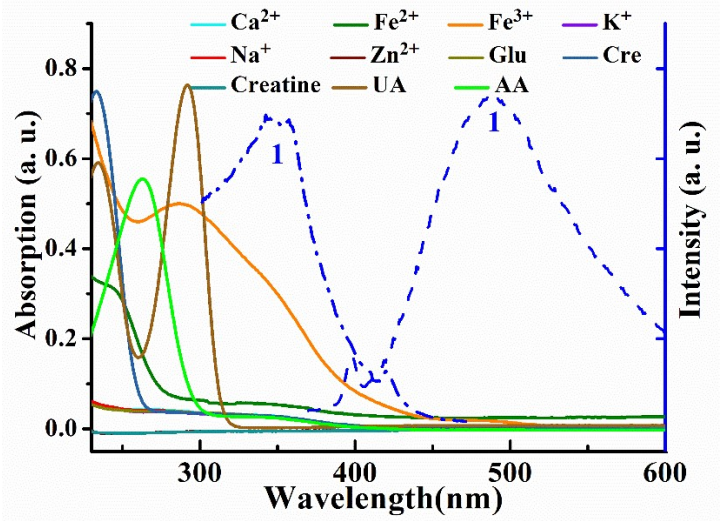

Fig. S11 UV-vis absorbance of the substances in the urine, together with the excitation and emission spectra of **1**.

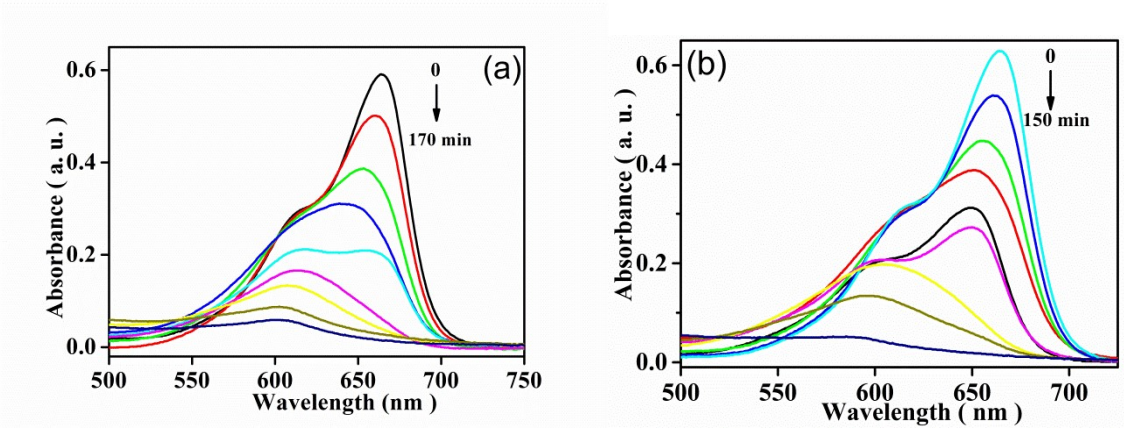

Fig. S12 Time-dependent UV-vis spectra of MB aqueous solution over **1** (a) and **3** (b) under UV light irradiation.

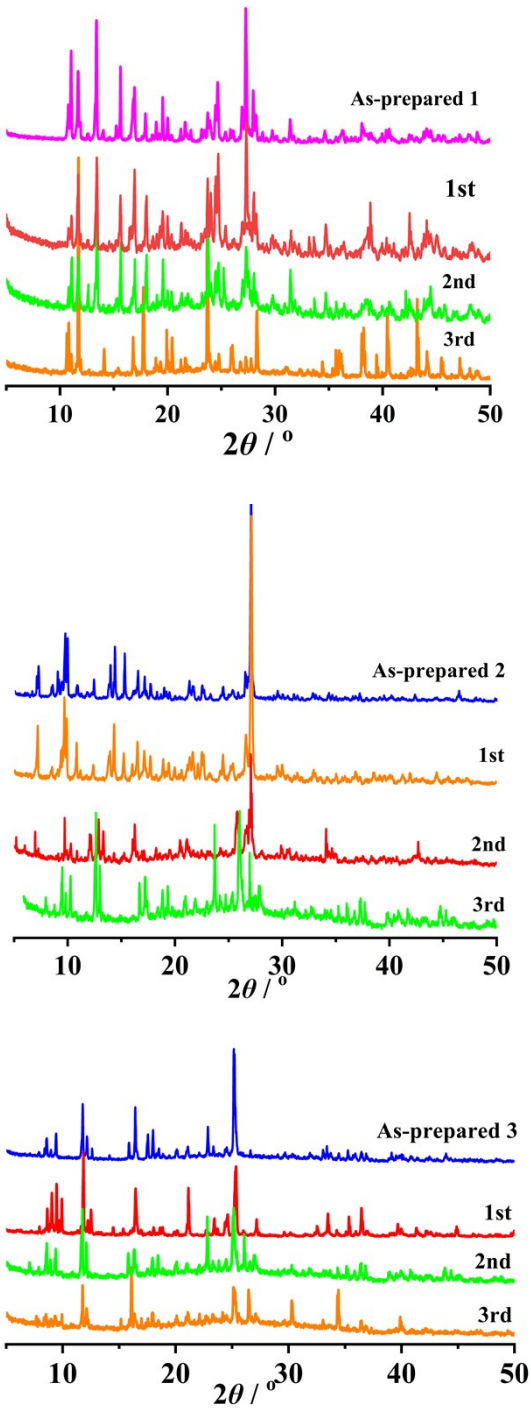

Fig. S13 PXRD patterns of **1**–**3** before and after each cycle of photocatalysis.

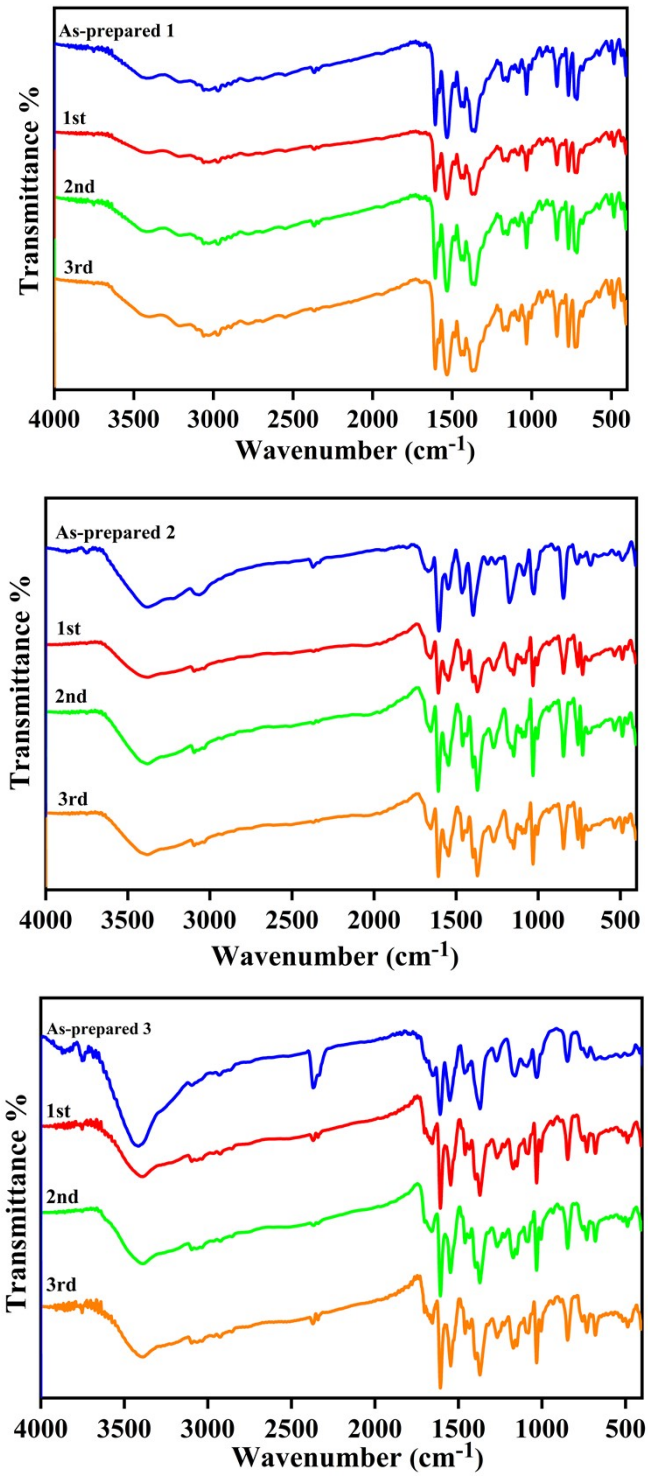

Fig. S14 FT-IR spectra of **1–3** after each cycle of photocatalysis.

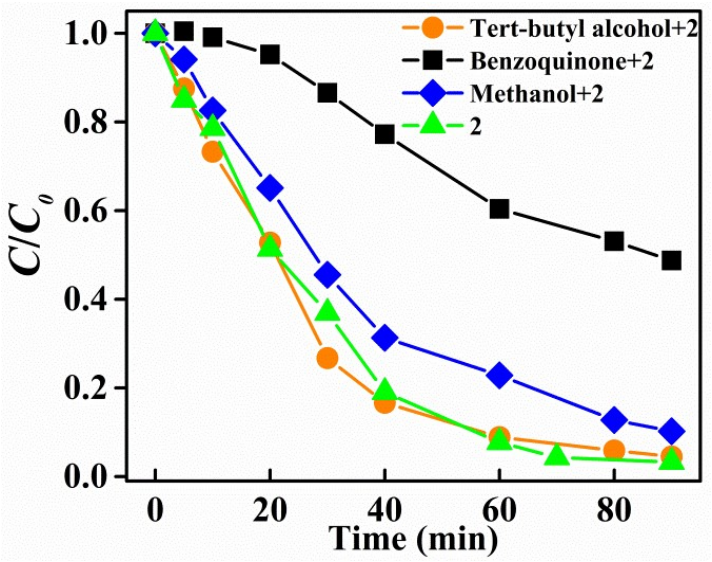

Fig. S15 Photodegradation efficiency of MB over **2** in the presence of different free radical scavengers.

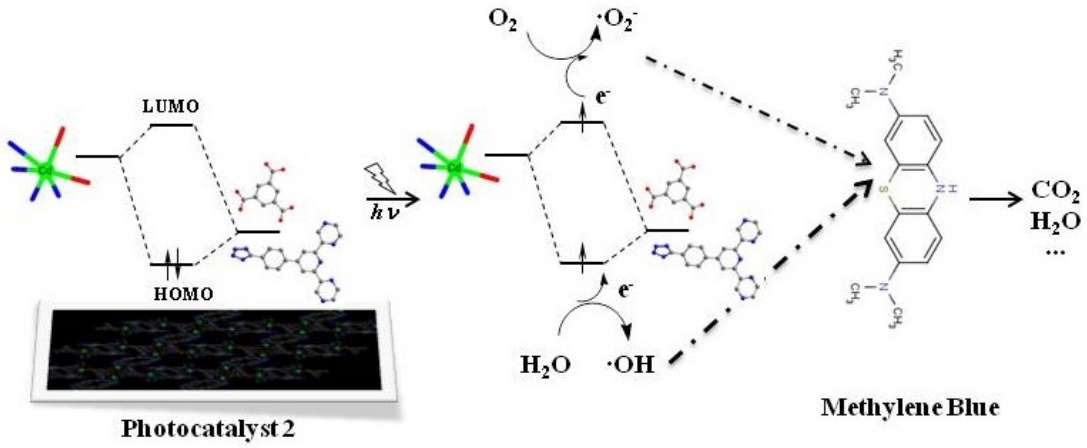

Fig. S16 A simplified model for the photocatalytic reaction mechanism over **2**.